European Journal of Inorganic Chemistry

Supporting Information

Stoichiometric and Catalytic Reduction of Carbon Dioxide by a Sterically Encumbered Amidinato Magnesium Hydride

Wimonsiri Huadsai, Laure Vendier, Helmar Görls, Lionel Magna, Sébastien Bontemps,* and Matthias Westerhausen*

General Experimental Section

1. Synthesis of amidine 1:

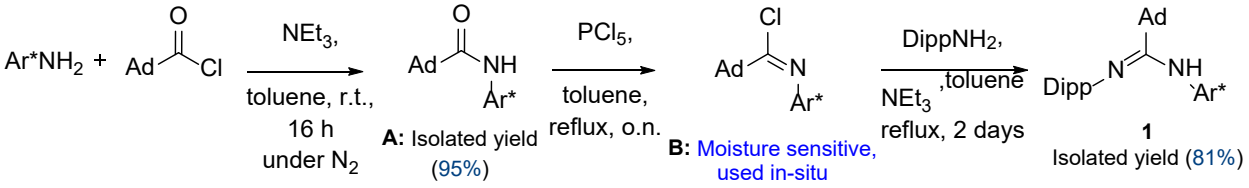

2,6-Dibenzhydryl-4-tolylamine (Ar^*NH_2) (40 g, 90.9 mmol) and 1-adamantane-carbonyl chloride (18 g, 90.6 mmol) were added to 250 ml of dichloromethane. Then, the distilled triethylamine, NEt_3, (18 ml, 129.8 mmol) was added dropwise to the solution mixture at room temperature. The reaction mixture was stirred at room temperature overnight, resulting in a white solid precipitate. The crude mixture was then quenched with 1 M of $NaHCO_3$ and washed with distilled water (2 x 50ml). The organic fraction was separated and dried over anhydrous $MgSO_4$. Volatiles were removed from the filtrate in vacuo to yield product **A** as a white powder (yield: 52 g, 95%). The characteristic signals of **A** in ^1H and $^{13}C\{^1H\}$ are consistent with the reported data.

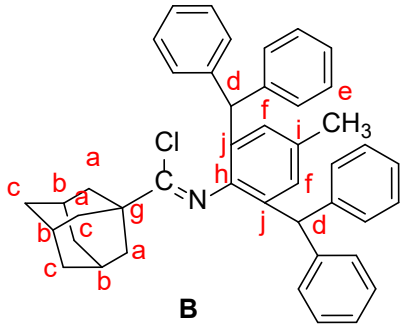

Compound **A** (20 g, 33.22 mmol) and phosphorus pentachloride, PCl_5, (9.68 g, 46.48) were combined in a 250 ml Schlenk flask. Then anhydrous toluene (150 ml) was added, and the reaction solution was heated at reflux overnight under nitrogen. The crude mixture was cooled to ambient temperature, and the solvent was removed in *vacuo* using a secondary trap to give white solid residues. After the removal of the solvent, the solid residues were heated to 150 °C for 2 h to remove unreacted PCl_5 and by-product $OPCl_3$. This procedure gave the moisture-sensitive white-brownish compound **B** that was not isolated. The full conversion of **A** to **B** was confirmed by ^1H NMR spectroscopy. Compound **B** was used directly without further purification.

In situ characterization of B:

^1H NMR (400 MHz, 298 K, C_6D_6): δ 1.51 (m, 6H, Ad–H^c), 1.81 (m, 6H, Ad–H^a), 1.83 (m, 3H, Ad–H^b), 1.88 (s, 3H, $CH_3{}^e$), 5.69 (s, 2H, CH^d–Ph_2), 6.91 (s, 2H, Ar–H^f), 7.06–7.09 (m, 8H, Ar–H), 7.13 (m, 8H, Ar–H), 7.28 (d, 4H, Ar–H).

$^{13}C\{^1H\}$ NMR (101 MHz, 298 K, C_6D_6): δ 21.2 (CH_3^e), 28.6 (Ad–C^b), 36.7 (Ad–C^c), 40.3 (Ad–C^a), 45.9 (Ad–C^{IV-g}), 52.5 (CH^d–Ph_2), 126.5, 126.7, 128.5, 128.6 (Ar–C), 129.7 (Ar–C^f), 130.4 (Ar–C), 133.0 (Ar–C^{IV-j}), 133.3 (Ar–C^{IV-i}), 143.2 (Ar–C^{IV-h}), 143.9 (Ar–C^{IV}), 155.1 (Cl–C=N).

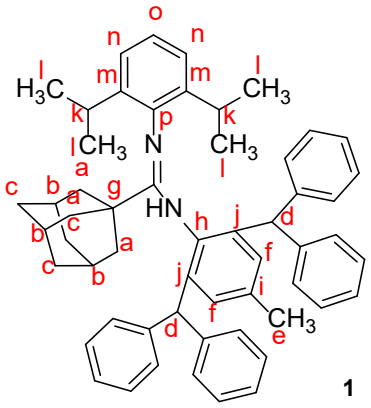

1

Compound **B** was combined with 2,6-diisopropylaniline (5.86 g, 33.32 mmol) in a Schlenk flask and dissolved in anhydrous toluene (100 ml). Triethylamine (6.20 ml, 44.32 mmol) was added subsequently to the solution in an inert atmosphere. The reaction was heated at reflux for 2 days, cooled to r.t., and quenched with 1 M aqueous $NaHCO_3$ (100 ml). The crude product was extracted with deionized water (2 x 50 ml) and separated in a separating funnel. The organic layer was dried over anhydrous $MgSO_4$, and all volatiles were removed in *vacuo*, yielding a sticky brownish product. The residues were then washed with MeOH (3 x 20 ml), yielding the compound as a white powder (20.3 g, 81%). A colorless crystal suitable for XRD analysis of **1** was obtained from hot ethanol.

Physical data of **1**: **^{1}H NMR** (400 MHz, 298 K, $CDCl_3$): δ 1.01 (d, $^3J_{HH}$ = 6.7 Hz, 6H, Dip–CH_3^l), 1.18–1.29 (m, 9H, Ad–H), 1.31 (d, overlapped with Ad–H^a peaks, $^3J_{HH}$ = 6.7 Hz, 6H, Dip–CH_3^l), 1.42 (m, 3H, Ad–H^b), 1.61 (m, 3H, Ad–H^c), 2.06 (s, 3H, CH_3^e), 3.28 (sept, $^3J_{HH}$ = 6.7 Hz, 2H, Dip–CH^k), 4.62 (s, 1H, NH), 5.95 (s, 2H, CH^d–Ph_2), 6.45 (s, 2H, Ar*Ar–H^f), 6.84 (m, 1H, Dip–Ar–H^o), 6.94 (m, 6H, Ar*Ar–H), 7.04 (m, 4H, Ar*Ar–H^o), 7.15 (m, 2H, Dip–Ar–H^n), 7.20–7.23 (m, 10H, Ar*Ar–H).

$^{13}C\{^1H\}$ NMR (100 MHz, 298 K, $CDCl_3$): δ 21.7 (CH_3^e), 22.5 (CH_3^l), 25.2 (CH_3^l), 28.5 (Dip–CH^k), 28.8 (Ad–C^c), 36.4 (Ad–C^b), 39.8 (Ad–C^a), 43.5 (Ad–C^{IV-g}), 52.7 (CH^d–Ph_2), 120.9 (Dip–Ar–C), 122.2 (Ar*Ar–C), 126.3 (Dip–Ar–C), 128.2 (Ar*Ar–C), 128.4 (Ar*Ar–CH), 129.4 (Ar*Ar–C), 129.6 (Ar–C^f), 130.6 (Ar*Ar–C), 135.6 (Ar*Ar–C^{IV-j}), 135.8 (Ar*Ar–C^{IV-i}), 137.1 (Dip–Ar–C^{IV-m}), 143.1 (Dip–Ar–C^{IV-p}), 144.3 (Ar*Ar–C^{IV}), 144.4 (Ar*Ar–C^{IV}), 145.8 (Ar*Ar–C), 155.6 (NCN).

M.p. 268-270 ºC.

Anal. calc. for $C_{56}H_{60}N_2$: C 88.37, H 7.95, N 3.68; **found**: C 88.32, H 7.91, N 3.63.

HRMS (ESI$^+$) m/z: calc. 760.48, **found**: 761.48 (**1**+H^+).

IR (solid, ν/cm^{-1}): 3448 (w, ν(N-H)), 3058 (w), 3023 (w), 2957 (w), 2906 (w), 2880 (w), 1613 (m), 1600 (m), 1583 (m), 1492 (m), 1475 (m), 1448 (m), 1430 (m), 1380 (w), 1359 (w), 1323 (w), 1292

(w), 1258 (w), 1227 (w), 1181 (w), 1157 (w), 1104 (w), 1076 (w), 1063 (w), 1043 (w), 1031 (w), 982 (w), 944 (w), 931 (w), 920 (w), 879 (w), 806 (w), 762 (m), 747 (m), 700 (s), 646 (w), 634 (m), 622 (w), 605 (w), 556 (w), 546 (w), 524 (w), 482 (w), 470 (w), 457 (w), 420 (w).

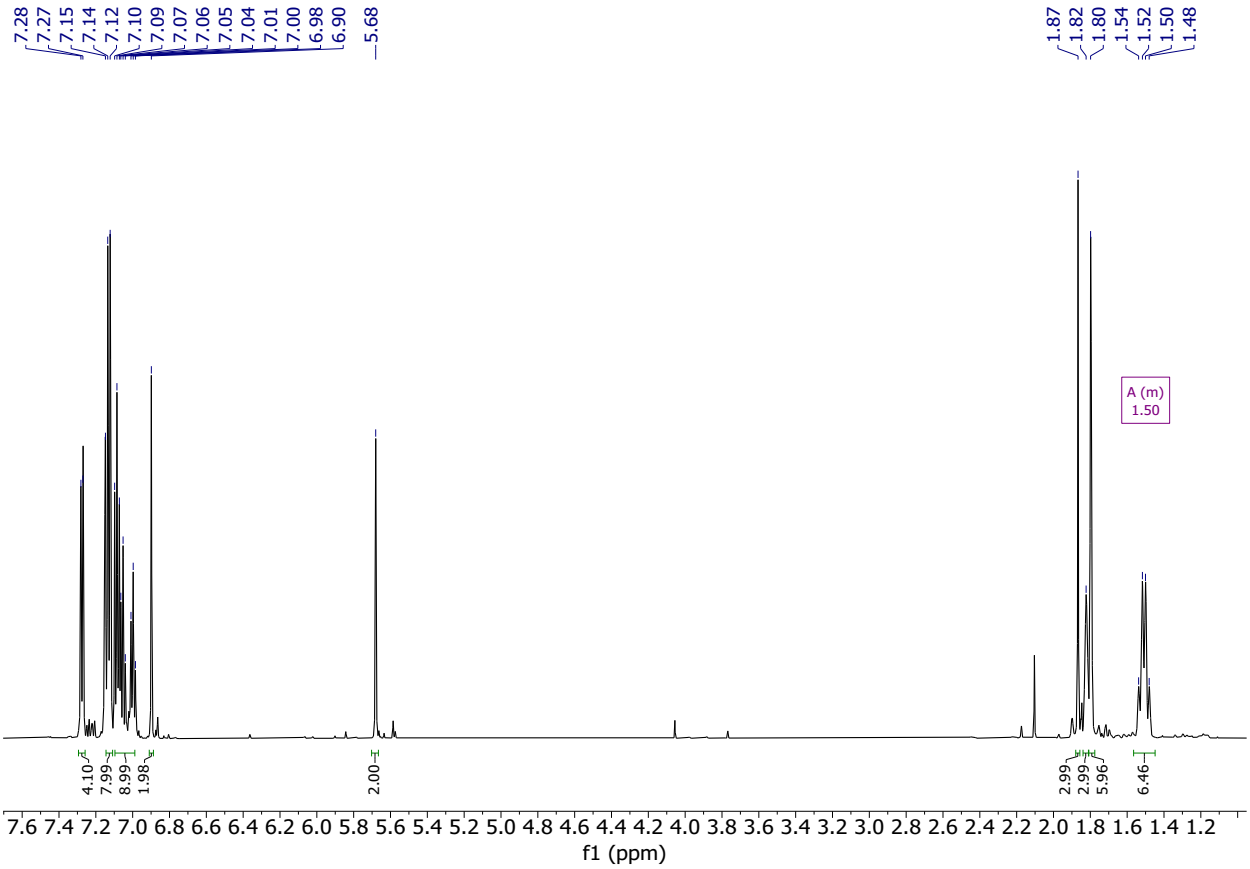

Figure S1: ^{1}H NMR spectrum of intermediate **B** (400 MHz, 298 K, C_6D_6).

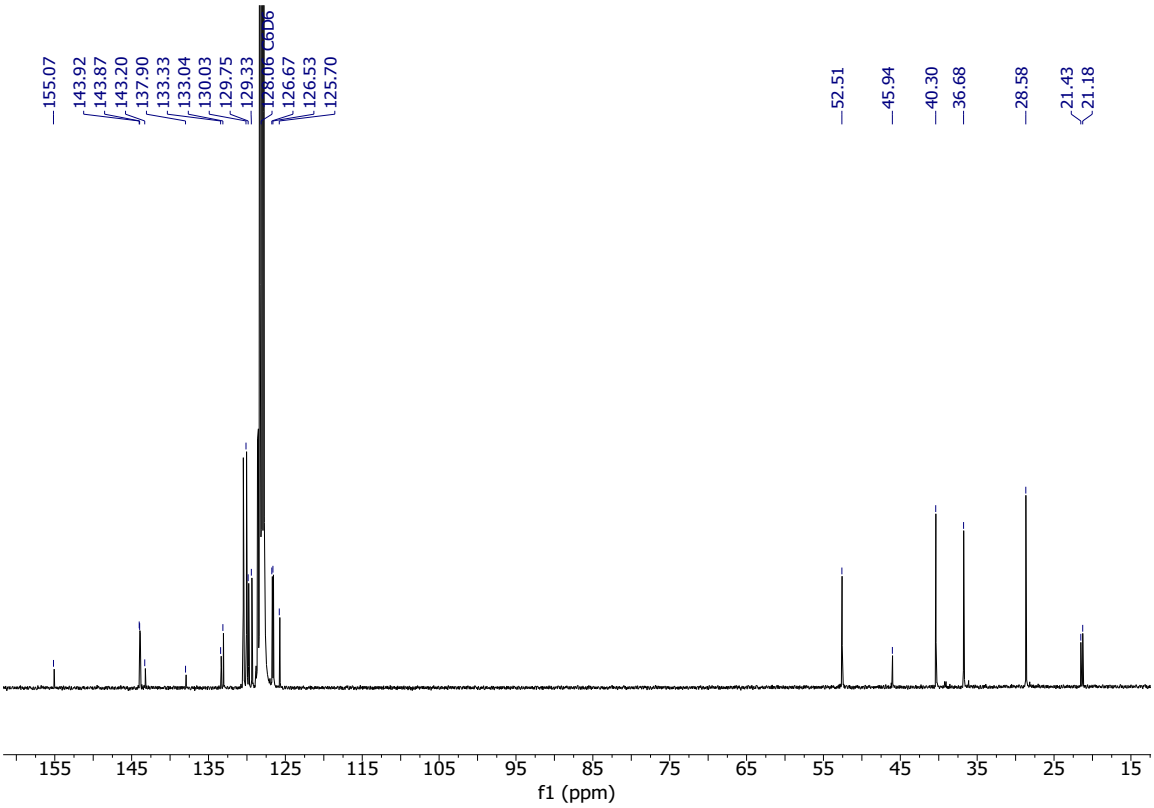

Figure S2: $^{13}C\{^{1}H\}$ NMR spectrum of intermediate **B** (101 MHz, 298 K, C_6D_6).

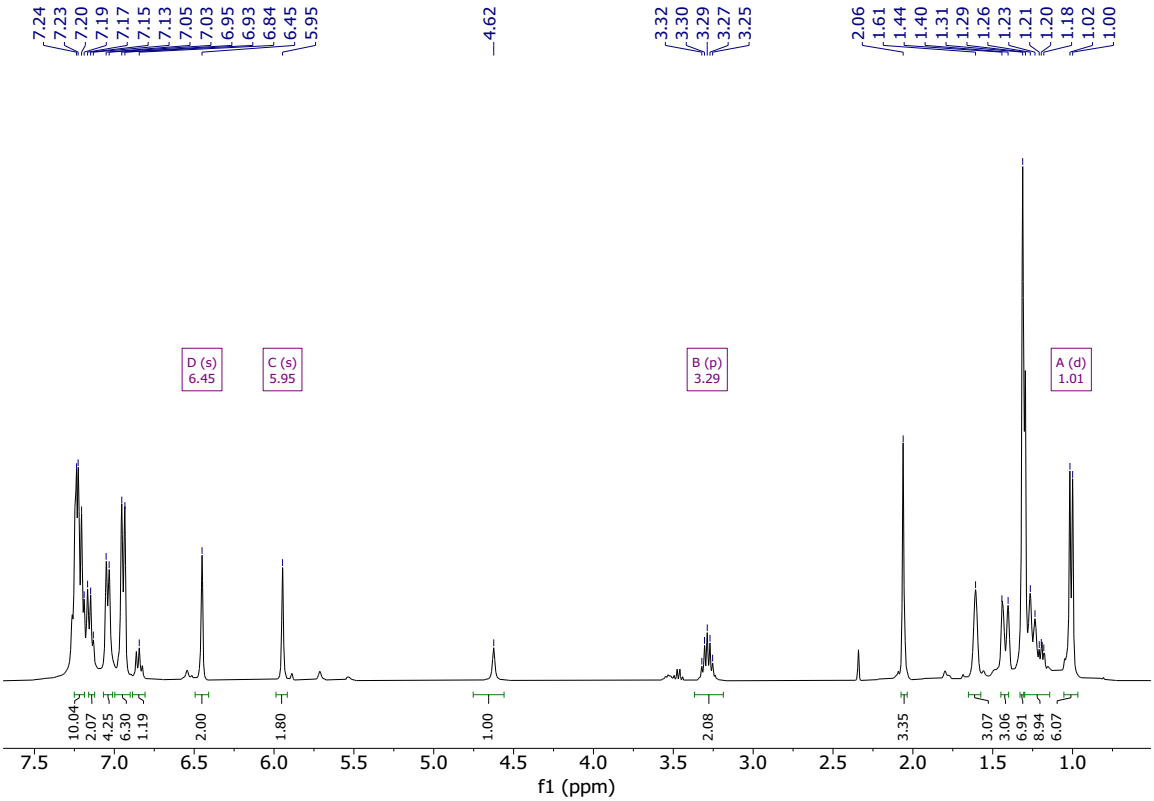

Figure S3: ^{1}H NMR spectrum of ligand **1** (400 MHz, 298 K, $CDCl_3$).

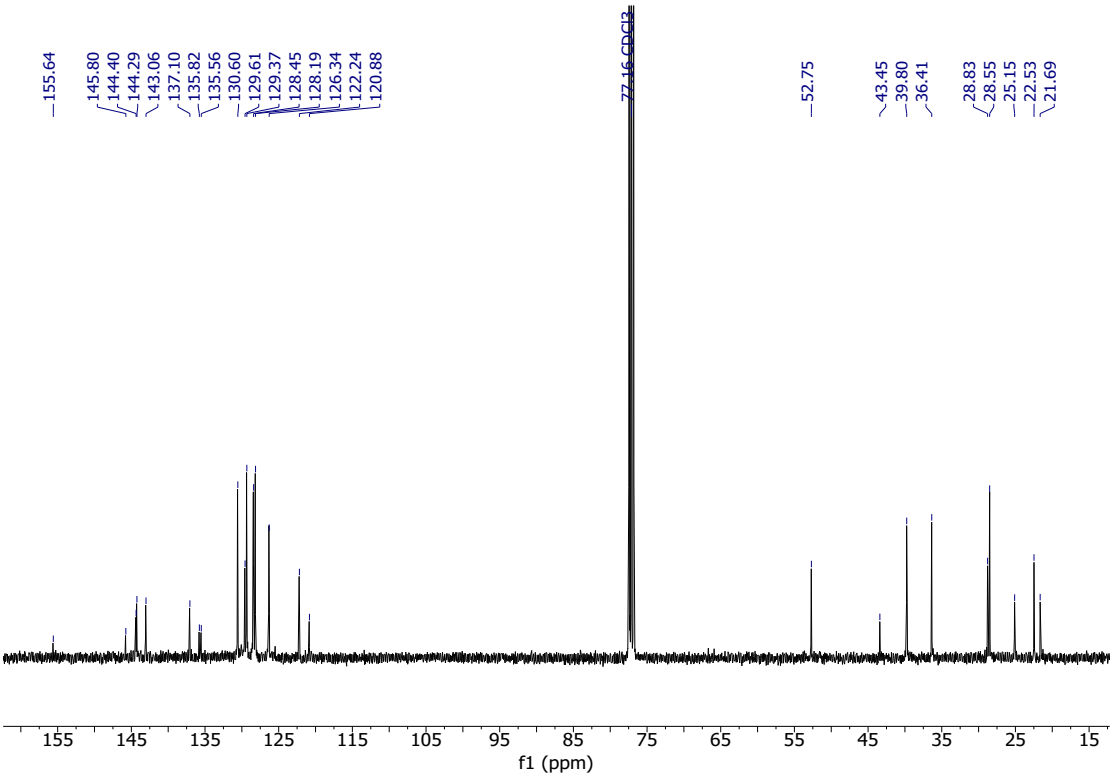

Figure S4: $^{13}C\{^{1}H\}$ NMR spectrum of ligand **1** (101 MHz, 298 K, $CDCl_3$).

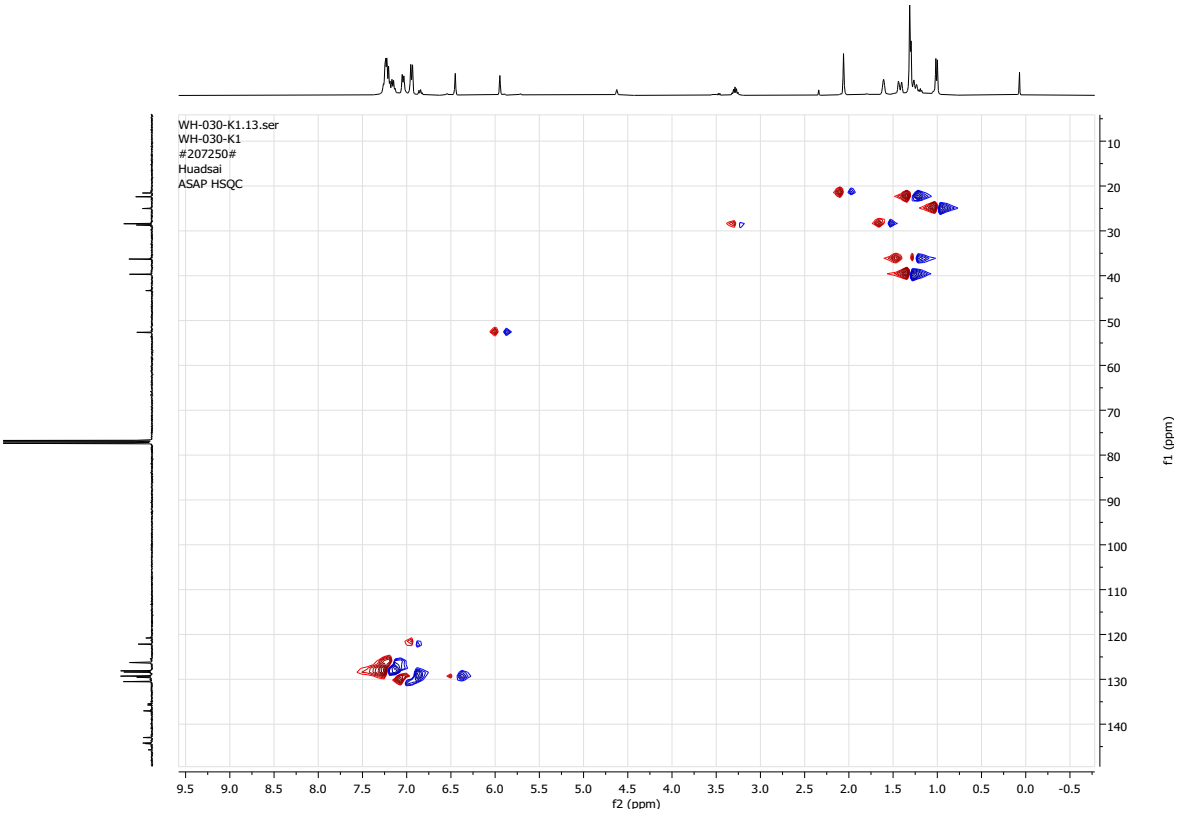

Figure S5: ^{1}H-^{13}C HSQC NMR spectra of **1** (400 MHz, 298 K, $CDCl_3$).

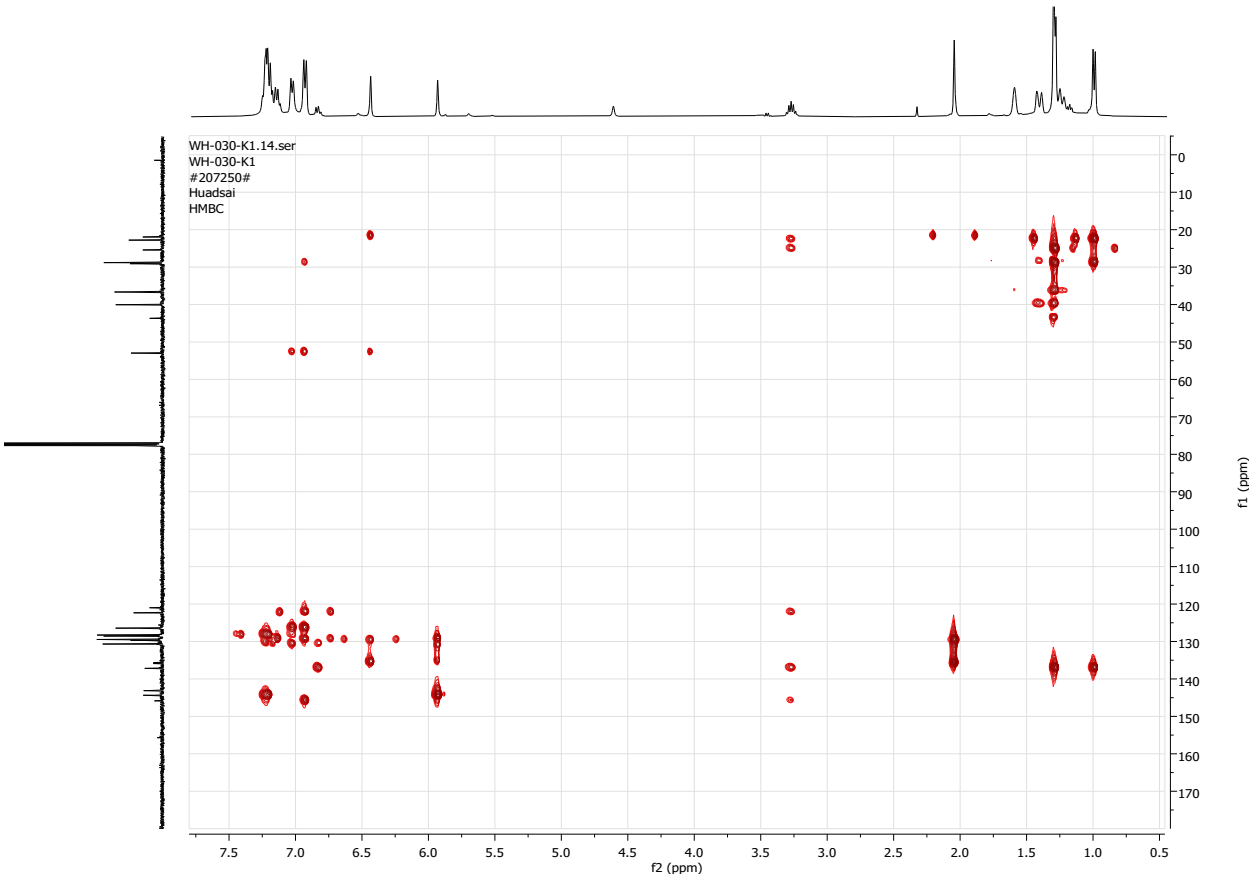

Figure S6: ^{1}H-^{13}C HMBC NMR spectra of **1** (400 MHz, 298 K, $CDCl_3$).

2. Synthesis of amidinato Mg hydride (3)

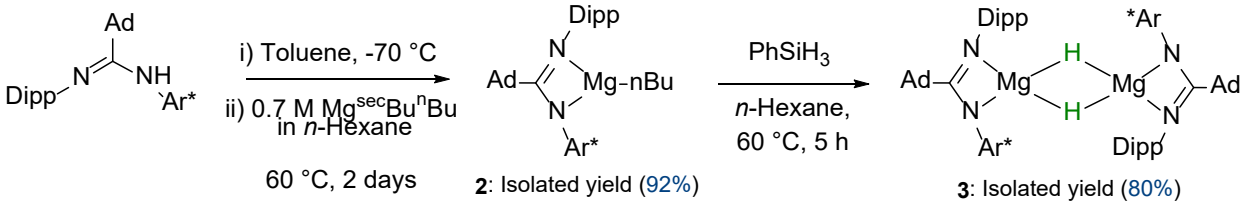

Numbering scheme for assignment of NMR signals:

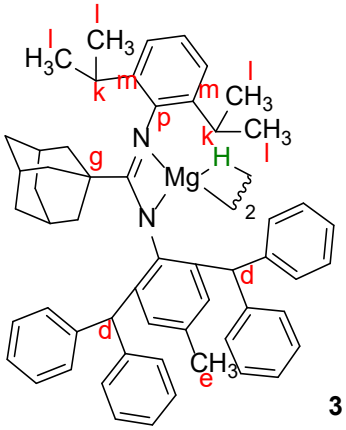

3

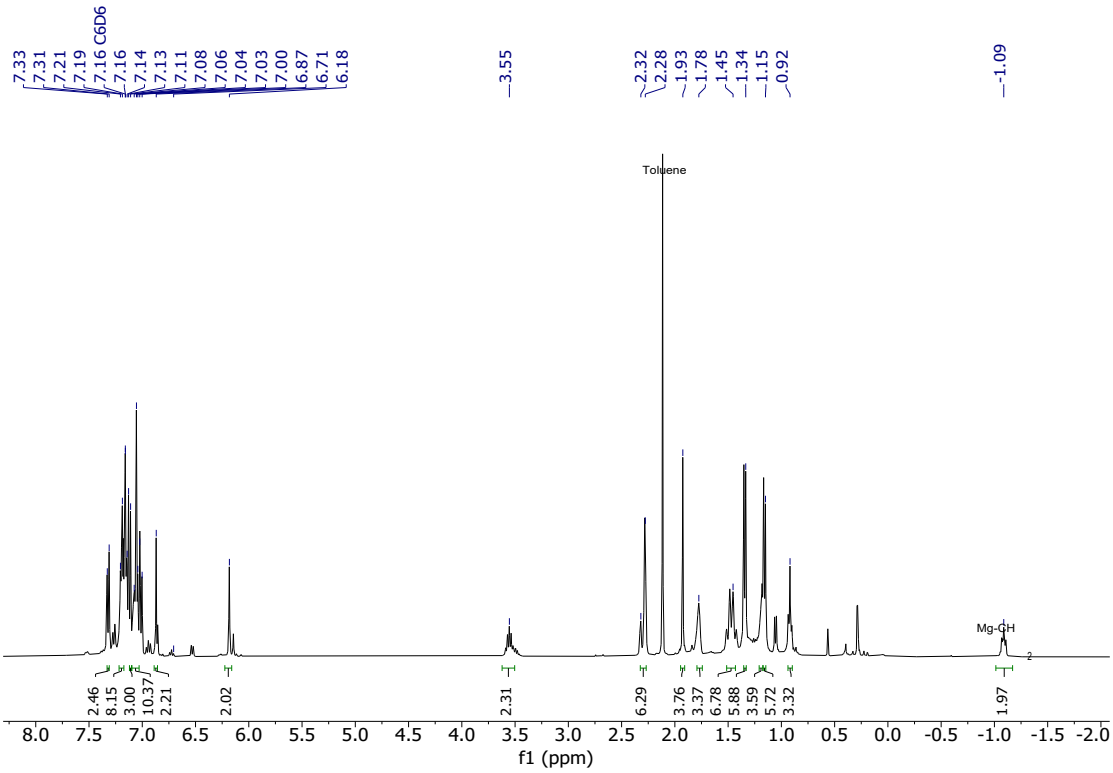

Figure S7: ^{1}H NMR spectrum of intermediate **2** [LMg(^{n}Bu)] (400 MHz, 298 K, C_6D_6).

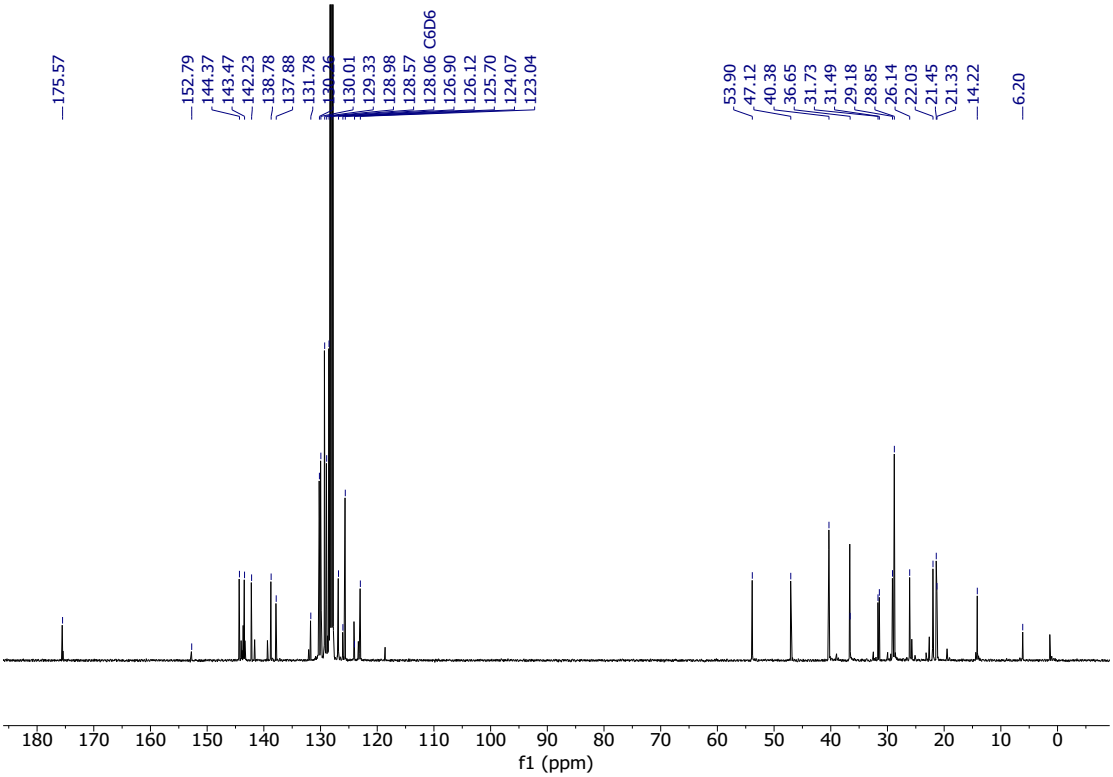

Figure S8: $^{13}C\{^{1}H\}$ NMR spectrum of intermediate **2** [LMg(^{n}Bu)] (101 MHz, 298 K, C_6D_6).

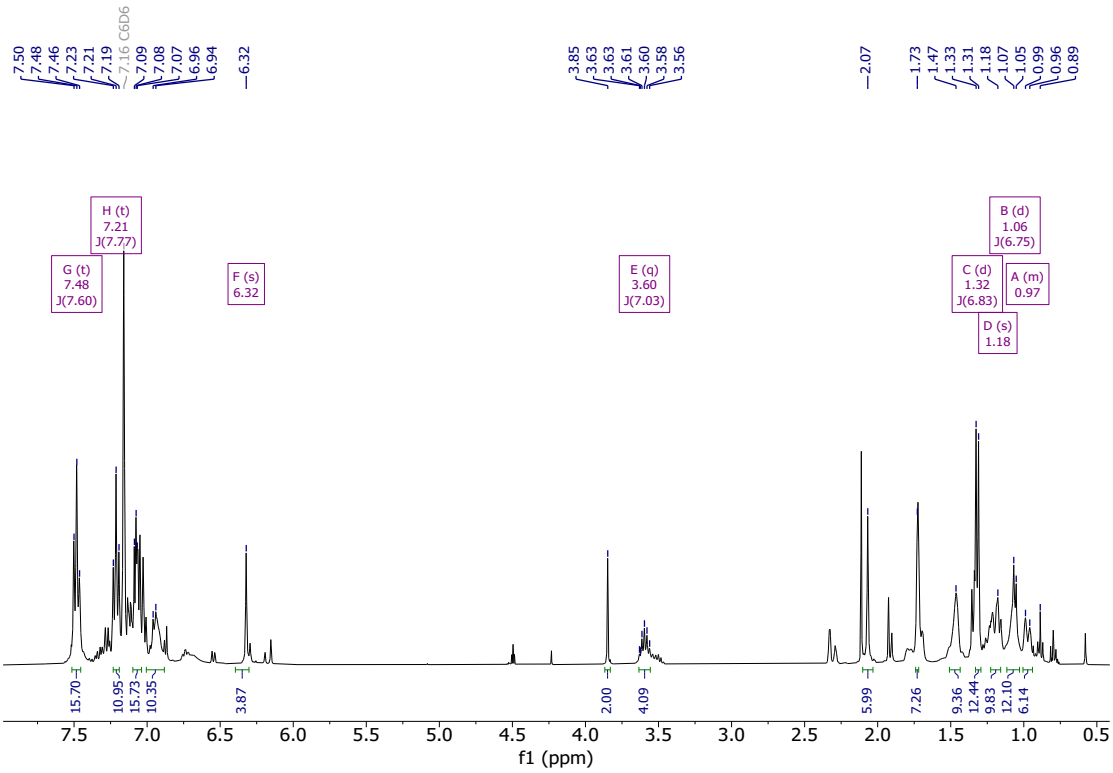

Figure S9*:* ^{1}H NMR spectrum of Mg compound **3** (400 MHz, 298 K, C_6D_6).

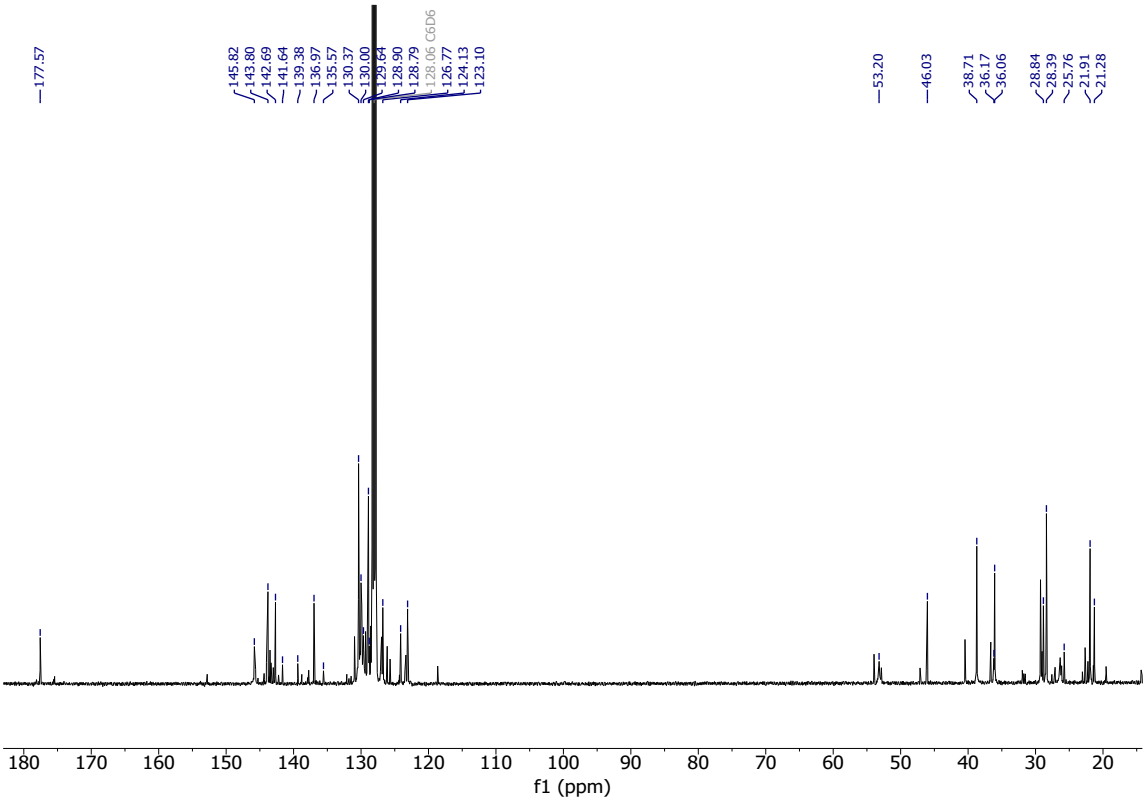

Figure S10: $^{13}C\{^{1}H\}$ NMR spectrum of Mg compound **3** (101 MHz, 298 K, C_6D_6).

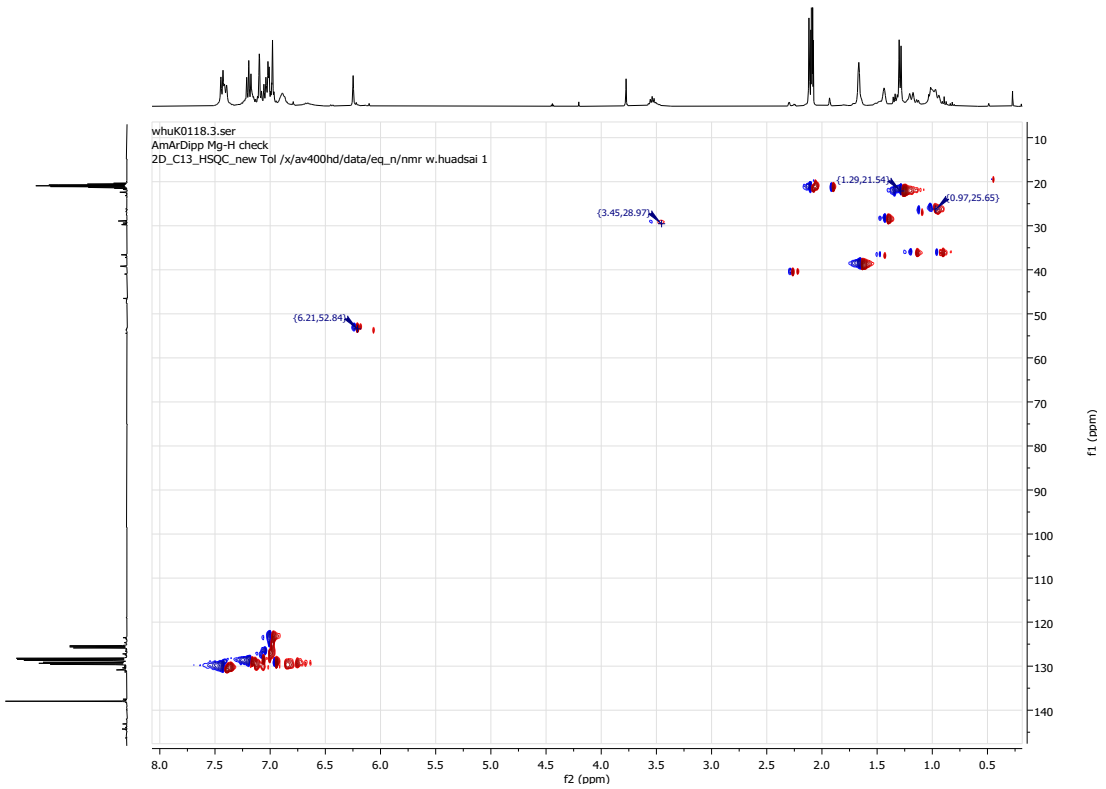

Figure S11: ^{1}H-^{13}C HSQC NMR spectra of [L^{Ad}Mg(μ-H)]$_2$ (**3**) (400 MHz, 298 K, toluene-d$_8$).

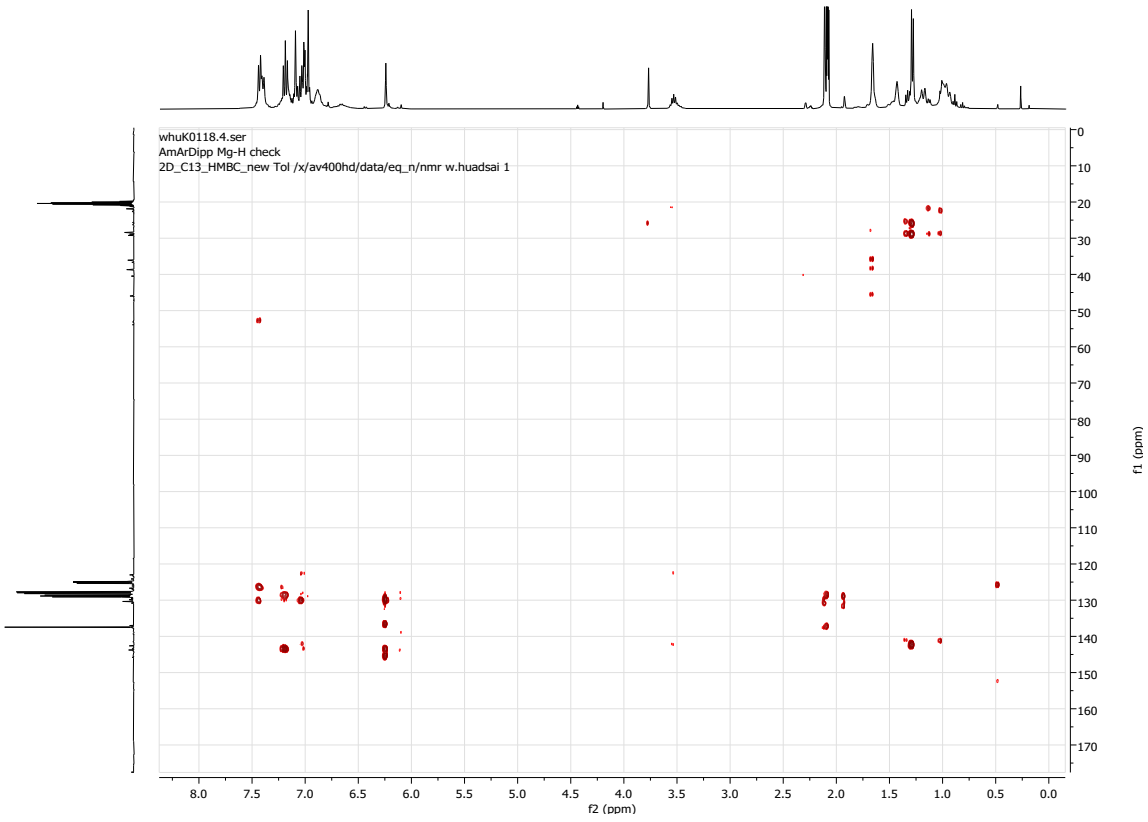

Figure S12: ^{1}H-^{13}C HMBC NMR spectra of [L^{Ad}Mg(μ-H)]$_2$ (**3**) (400 MHz, 298 K, Toluene-d$_8$).

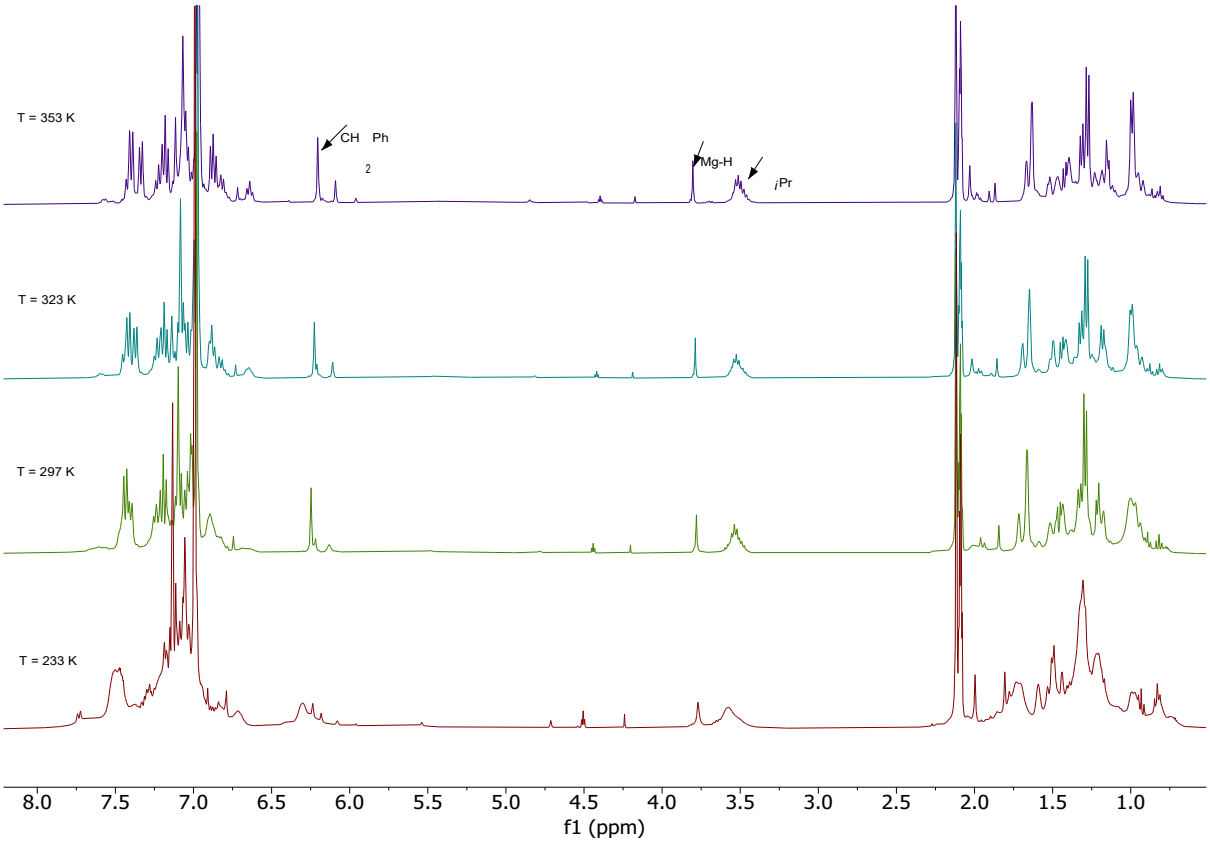

Figure S13: ^{1}H NMR stacked spectra of complex **3** at different temperatures (from top to bottom: 353 K to 233 K) (400 MHz, 298 K, toluene-d_8). The stacked spectra do not show any appreciable temperature dependency of the hydride chemical shift.

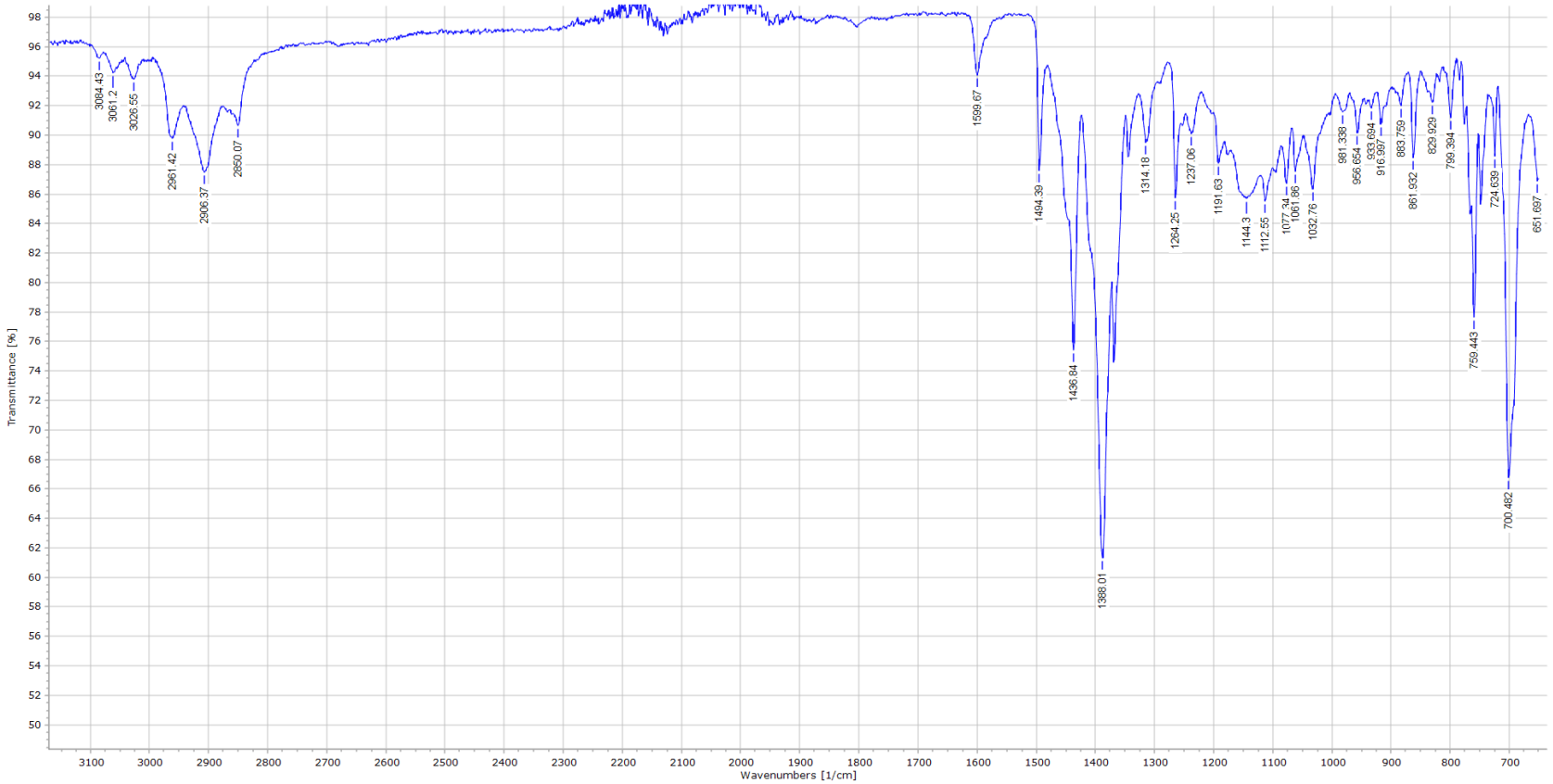

Figure S14: IR spectrum in solid state of the amidinato magnesium hydride complex **3**.

3. Reaction of amidinato Mg hydride 3 with CO_2

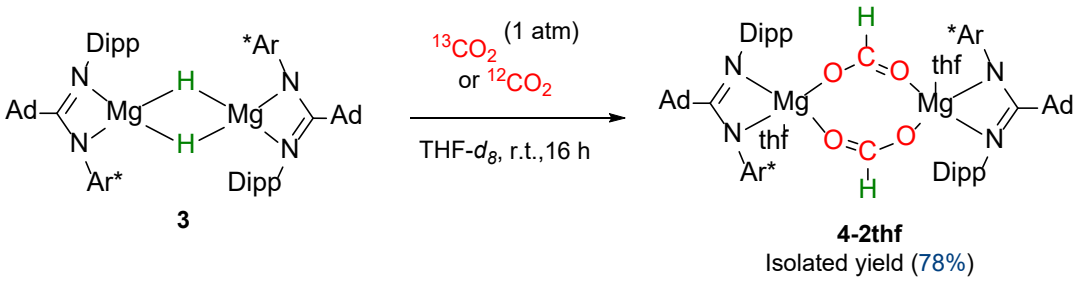

Numbering scheme for the assignment of the NMR signals:

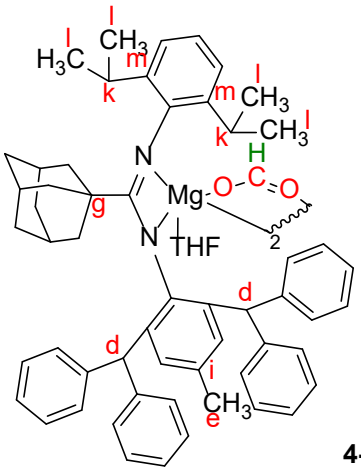

4-2thf

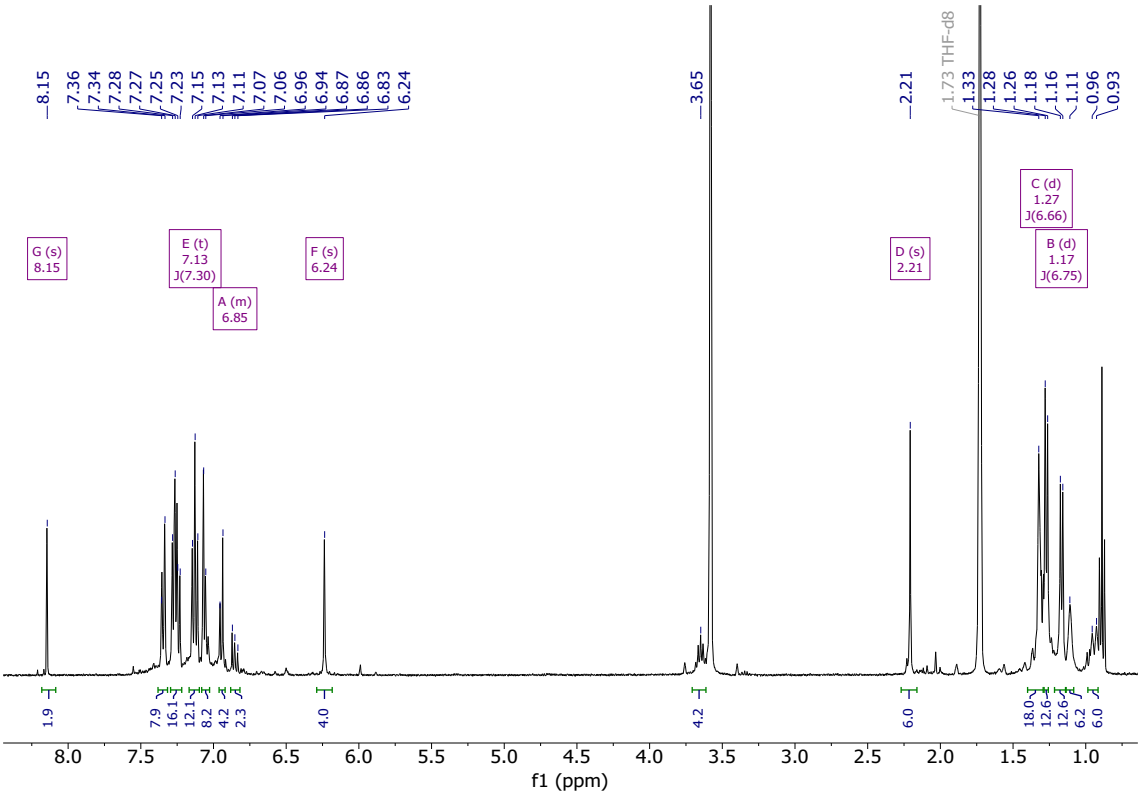

Figure S15: ^{1}H NMR spectrum compound **4-2thf** (400 MHz, 298 K, THF-d_8).

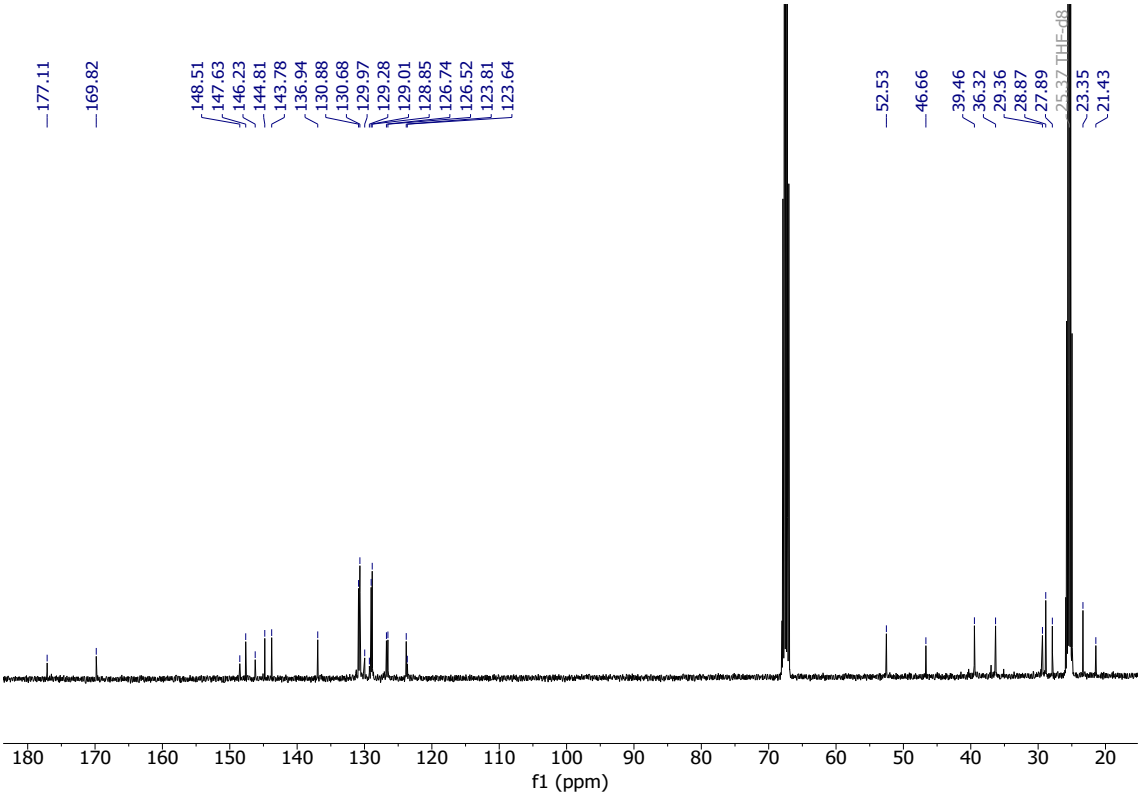

Figure S16: ^{13}C{^{1}H} NMR spectrum of compound **4-2thf** (100 MHz, 298 K, THF-d_8).

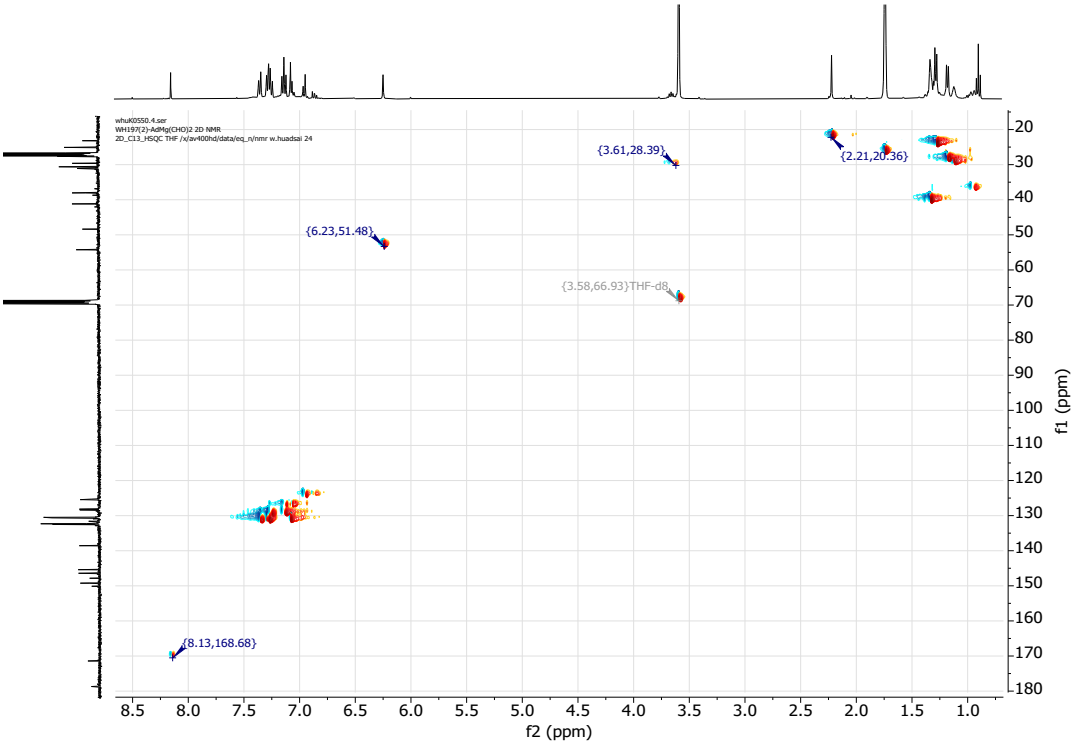

Figure S17: ^{1}H-^{13}C HSQC NMR spectrum of **4-2thf** (400 MHz, 298 K, THF-d_8).

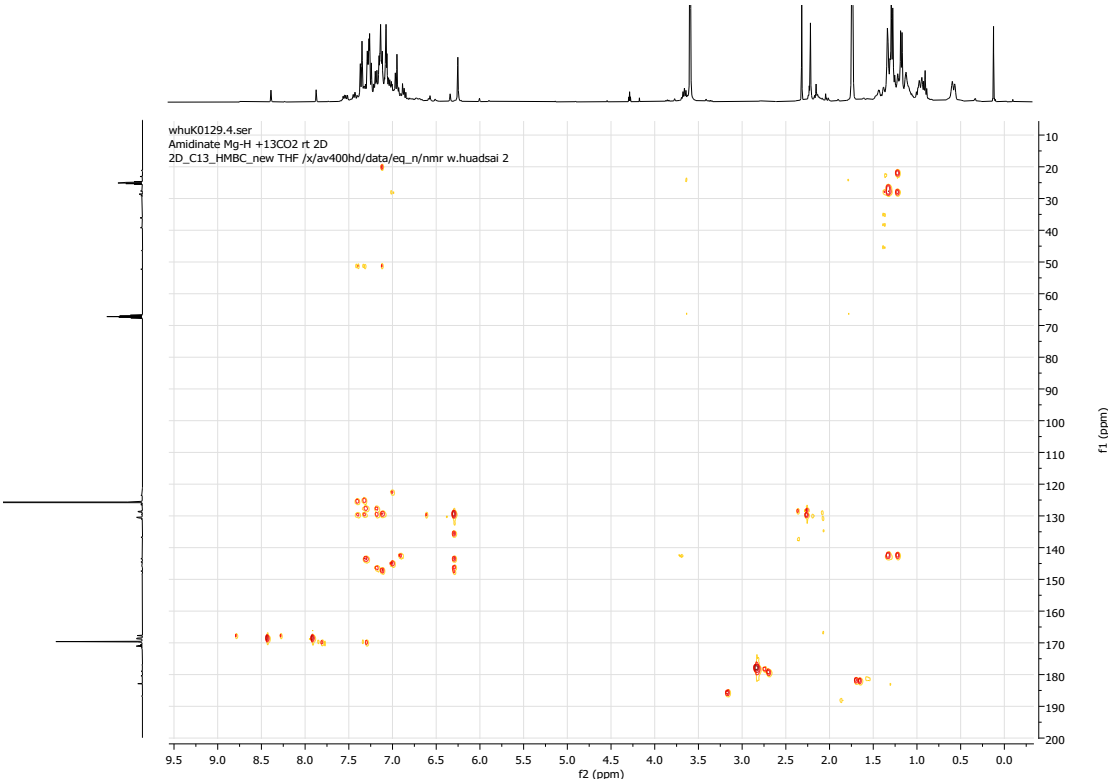

Figure S18: ^{1}H-^{13}C HMBC NMR spectra of **4-2thf** (400 MHz, 298 K, THF-d_8).

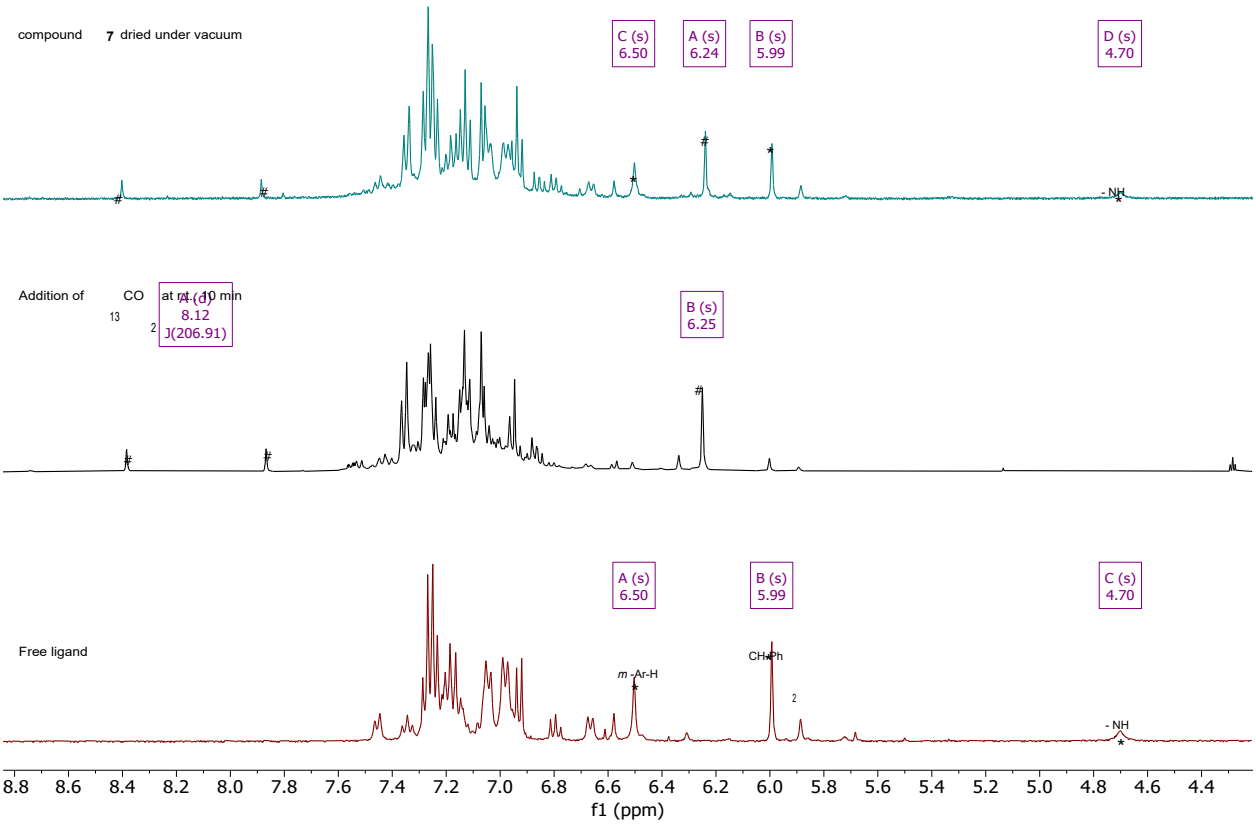

Figure S19: Stacked ^{1}H NMR spectra, exhibiting the decomposition of compound **4-2thf** under vacuum (400 MHz, 298 K, THF-d_8). From bottom to top: i) characteristic signals corresponding to amidinate ligand; ii) the generation of compound **4-2thf** after 10 min at r.t., showing the resonances of formate moiety; iii) compound **4-2thf** after applying high vacuum for 1 h at room temperature, leading to the decomposition and formation of free ligand **1**. The signals corresponding to free ligand are marked with asterisks (*) and complex **4-2thf** with #, respectively.

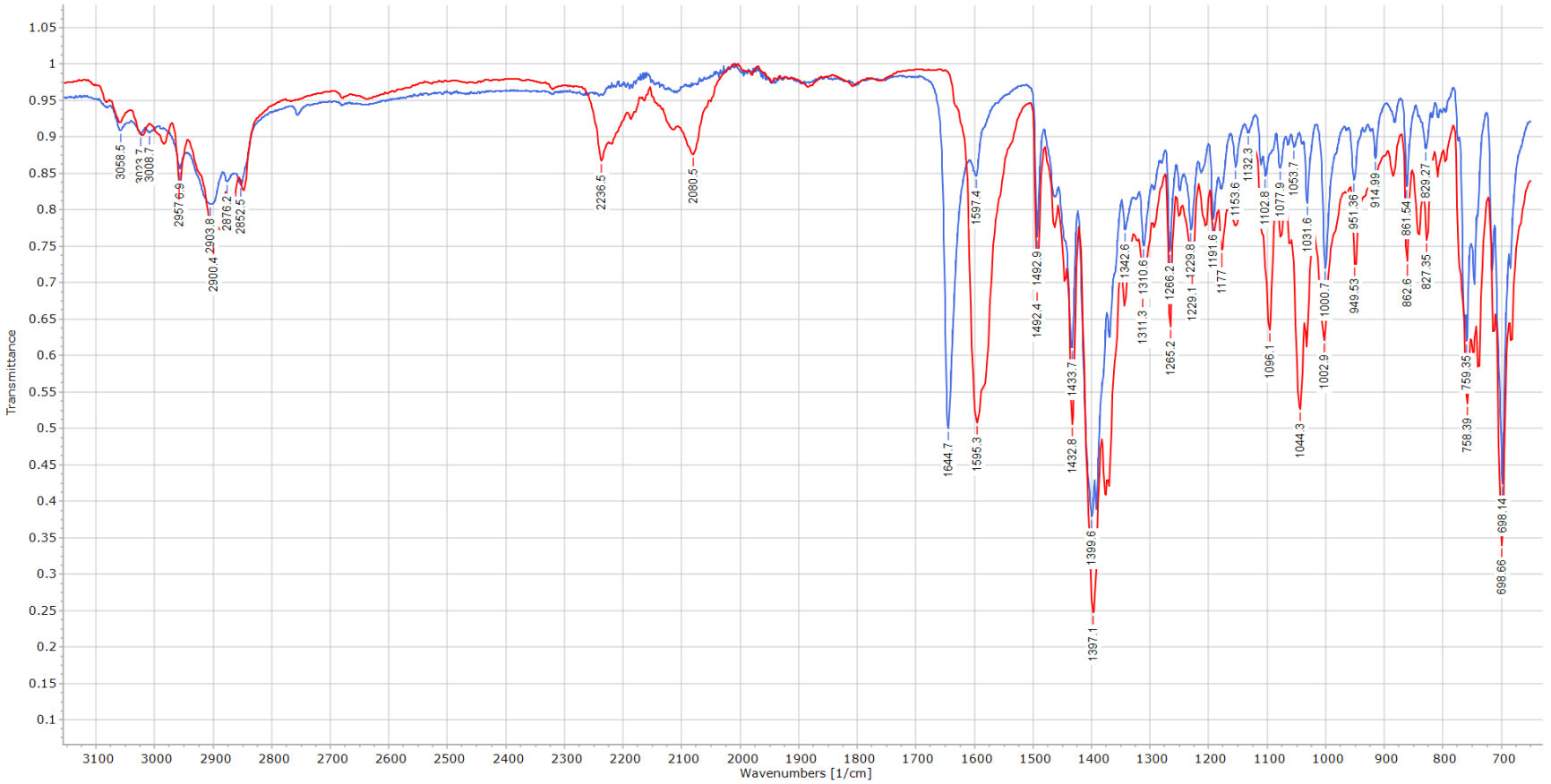

Figure S20: IR spectra in solid state of amidinate magnesium formate complex **[^{13}C]4-2thf** (red), **[^{12}C]4-2thf** (blue).

Table S1: Measured diffusion constants, calculated hydrodynamic radii in solution and solid state, and average molecular sizes in the solution for complexes.

Complex	**Experimental**		**Calculated**	**Estimated structure in solution**
	Diffusion Coefficient (x 10^{-10} m^2s^{-1})[a]	**Hydrodynamic radius (r_H) Å in solution**[b]	**Hydrodynamic radius (r_H) Å in solid state**[c]	
3[d]	3.8	9.7	8.2[f]	dimer
3[e]	5.8	7.5	-	monomer-dimer?
4-thf	4.4	9.9	9.3	dimer

[a] The diffusion coefficients were determined by regression analysis by fitting the peak areas to the Stejskal-Tanner equation from T1/T2 analysis module in Topspin 4.1.4 software. [b] r_H = hydrodynamic radius. The Diffusion coefficient and hydrodynamic radii are correlated theoretically by the Stokes-Einstein relation ($D= (kT)/(6\pi\eta rH)$) [c] Calculated from X-ray structure data under the assumption of spherical shape. [d] The D values were obtained from **3** measured in toluene-d_8. [e] The D values were obtained from **3** measured in THF-d_8. [f] The data was extrapolated from X-ray diffraction data of crystal **3-thf**. The $r_{(X\text{-}ray)}$ of ligand $L^{Ad}H$ were calculated at 6.4 Å as monomer in solid-state. The calculations of hydrodynamic radii in THF-d_8 and toluene-d_8 were done by using the viscosity values of η = 5.01 x 10^{-4} and 6.04 x 10^{-4} kg $m^{-1}s^{-1}$ at 293 K, respectively.

4. Crystallographic data

Table S2: Crystal data and refinement details for the X-ray structure determinations.

Compound	**1**	**3-thf**	**4-2thf**
formula	$C_{56}H_{60}N_2$	$C_{116}H_{124}Mg_2N_4O$	$C_{122}H_{134}Mg_2N_4O_6$[*]
fw ($g \cdot mol^{-1}$)	761.06	1638.80	1800.95[*]
T/°*C*	-140(2)	-173(2)	-173(2)
crystal system	monoclinic	triclinic	triclinic
space group	P 2_1/c	P $\bar{1}$	P $\bar{1}$
a/ Å	17.5669(5)	12.1321(3)	13.953(6)
b/ Å	11.3120(3)	12.9892(2)	15.403(6)
c/ Å	22.0746(5)	30.5910(5)	17.391(7)
α/°	90	95.1640(10)	83.436(14)
β/°	92.767(2)	92.478(2)	67.097(13)
γ/°	90	102.621(2)	75.517(15)
V/Å^3	4381.5(2)	4675.32(16)	3333(2)
Z	4	2	1
ρ ($g \cdot cm^{-3}$)	1.154	1.164	0.897[*]
μ (cm^{-1})	0.66	6.3	0.63[*]
measured data	21779	58517	72840
data with I > 2σ(I)	6000	11601	8845
unique data (R_{int})	8294/0.0645	15815/0.0520	12923/0.0726
wR_2 (all data, on F^2)[a)]	0.1881	0.1757	0.1685
R_1 ($I > 2\sigma(I)$) [a)]	0.0842	0.0593	0.0585
s [b)]	1.111	1.040	0.991
Res. dens./$e \cdot Å^{-3}$	1.259/-0.276	0.897/-0.574	0.706/-0.241
absorpt method	multi-scan	multi-scan	multi-scan
absorpt corr $T_{min}/_{max}$	0.6721/0.7456	0.76684/1.00000	0.6950/0.7457
CCDC No.	2334211	2334212	2334213

[*] derived parameters do not contain the contribution of the disordered solvent.

[a)] Definition of the *R* indices: $R_1 = (\Sigma \,||F_o| - |F_c||)/\Sigma |F_o|$;
$wR_2 = \{\Sigma[w(F_o^2-F_c^2)^2]/\Sigma[w(F_o^2)^2]\}^{1/2}$ with $w^{-1} = \sigma^2(F_o^2) + (aP)^2+bP$; $P = [2F_c^2 + Max(F_o^2]/3$;

[b)] $s = \{\Sigma[w(F_o^2-F_c^2)^2]/(N_o-N_p)\}^{1/2}$.

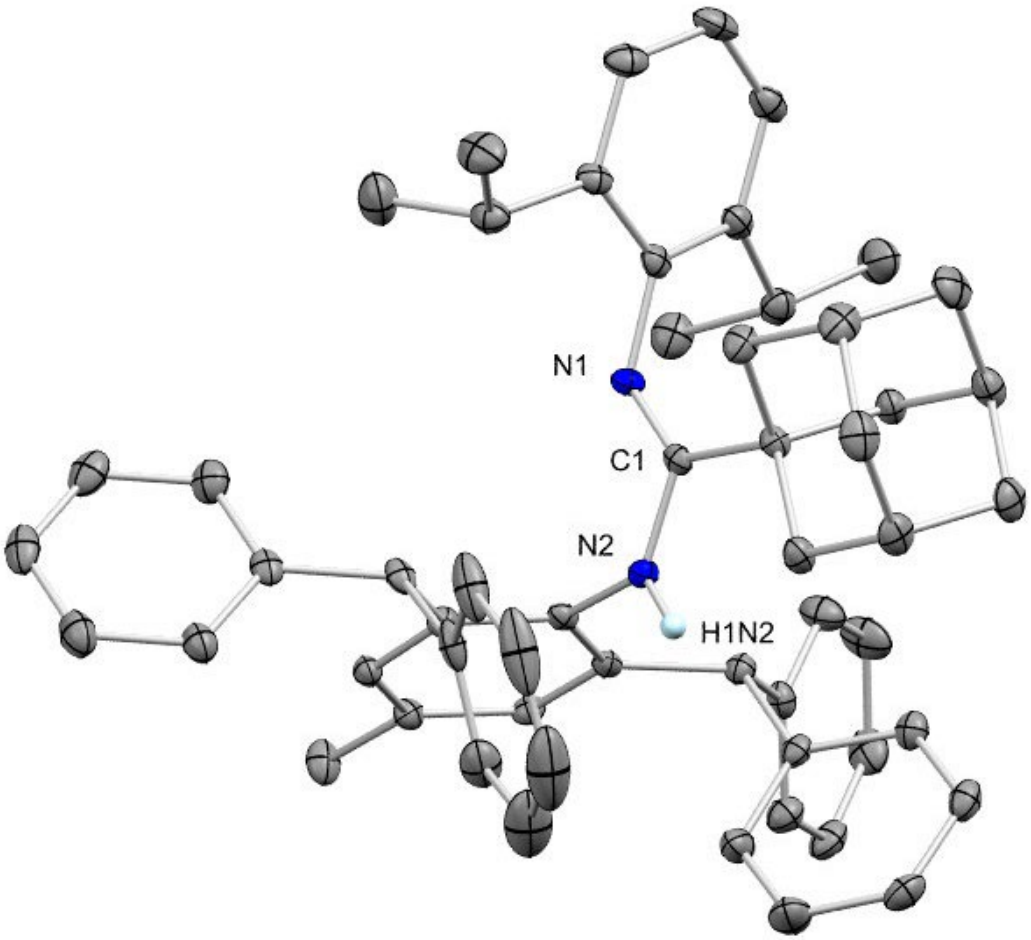

Figure S21: ORTEP representation of the molecular structure of pro-ligand amidine **1** with selective atom labeling. Displacement ellipsoids are set at 50% probability; hydrogen atoms are omitted for clarity. Selected bond lengths (Å): N1−C(1), 1.291(4); N2−C(1), 1.364(4); N1−H(1)−N2, 0.84(3). Selected bond angles (°): N−C(1)−N2, 117.4(3).

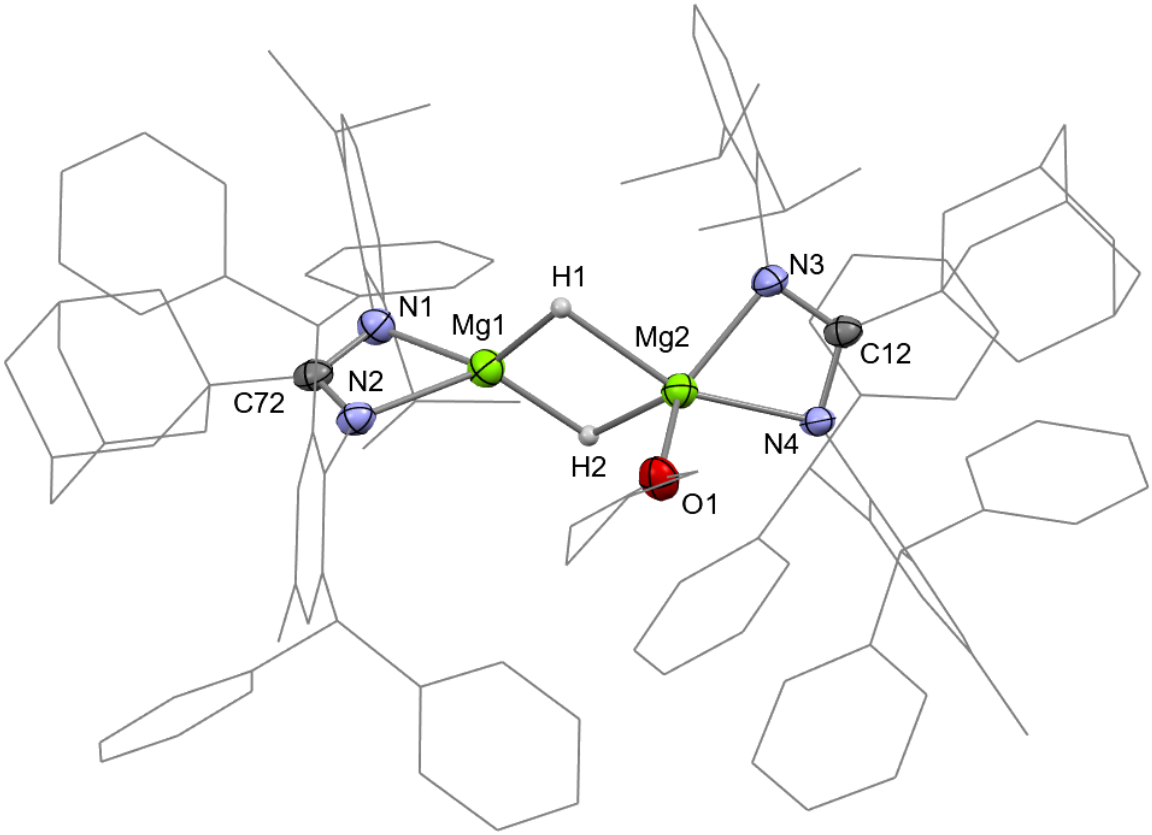

Figure S22: ORTEP representation of the molecular structure of **3-thf** with selected atom labeling. Displacement ellipsoids are set at 50% probability; hydrogen atoms except for the hydride protons H(1) and H(2) are omitted for clarity. The 2,6-*i*$Pr_2C_6H_3$ and 2,6-bis(diphenylmethyl)-4-methylphenyl moieties, adamantly and THF coordinated parts, have been set as wireframes for clarity reasons. Selected bond lengths (Å): Mg1−Mg2, 2.8533(12); Mg1−N(1), 2.046(2); Mg1−N(2), 2.087(2); Mg1−H(1), 1.8454(9); Mg1−H(2), 1.8842(8); Mg2−N(3), 2.049(2); Mg2−N(4), 2.142(2); Mg2−O(1), 2.0801(19); Mg2−H(1), 2.1816(8); Mg2−H(2), 1.9119(9). Selected bond angles (°): H(1)−Mg1−H(2), 91.38(4); H(1)−Mg2−H(2), 81.09(3); N(1)−Mg1−N(2), 64.55(8); N(3)−Mg2−N(4), 63.34(8).

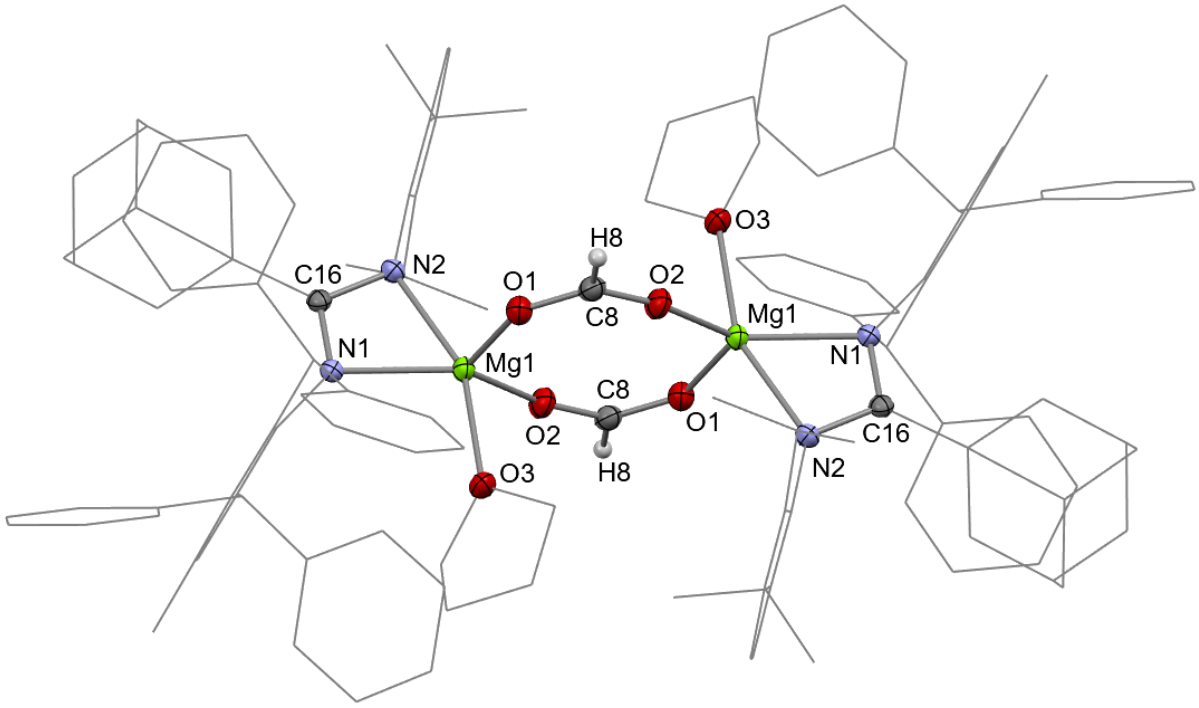

Figure S23: ORTEP representation of the molecular structure of **4-2thf** with selected atom labeling. Displacement ellipsoids are set at 50% probability; hydrogen atoms except for the formate protons are omitted for clarity. The 2,6-$iPr_2C_6H_3$ and 2,6-bis(diphenylmethyl)-4-methylphenyl moieties, adamantyl and THF-coordinated parts, have been set as wireframes for clarity. Selected bond lengths (Å): Mg1−N(1), 2.096(2); Mg1−N(2), 2.162(2); Mg1−O(1), 1.961(2); Mg1−O(2), 1.9404(19); Mg1−O(3), 2.1349(18); O1−C(8), 1.245(3); O2−C(8), 1.242(3). Selected bond angles (°): N(1)−Mg−N(2), 61.88(7); O(1)−Mg−O(2), 112.44(8); O(2)−Mg−N(2), 101.59(8); O(1)−Mg−N(2), 103.79(8); N(1)−Mg−O(3), 95.27(8); O(1)−Mg−O(3), 88.59(8); O(1)−Mg−N(1), 113.24(8). Symmetry operations: (i) −x+2, −y+1, −z+1.

5. Catalysis

5.1. Catalytic hydroboration of CO_2

In a glove box, Mg hydride complex **3** (1 mol%, 0.013 mmol), 9-BBN (0.13 mmol), and hexamethylbenzene as internal standard were dissolved in THF-d_8 (0.65 ml) in a vial. The solution was transferred to a pressurized NMR tube, which was sealed and removed from the glovebox. The NMR tube was first degassed and placed under 1 atm of CO_2 for 3 min. ^{1}H and ^{13}C{^{1}H} NMR analysis was performed every 10 minutes at 298 K. Product yields and the consumption of hydroborane were calculated by ^{1}H NMR integral against the internal standard.

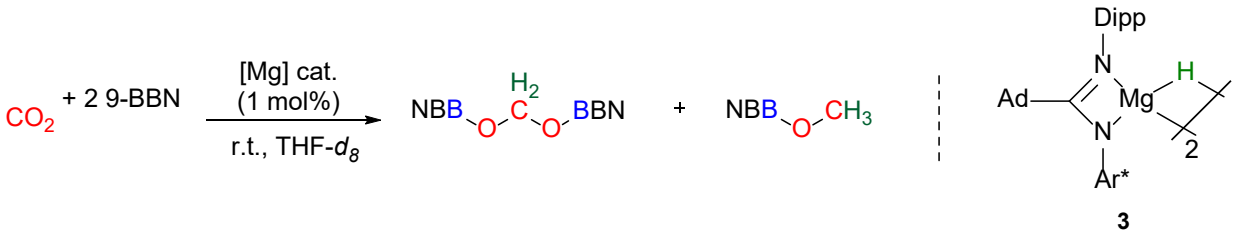

Table S3: Hydroboration of CO_2 to BBA^{BBN} are catalyzed by amidine Mg **1**.

Catalyst	Time	Yield of BBA (%)	TON (TOF)/ h^{-1}	Yield of R_2BOCHO (%)	Yield of R_2BOCH_3 (%)	Conversion of HBR_2 (%)
1	16 h	76	76 (8)	-	22	97

[a] Reaction conditions: 1 atm CO_2, 0.13 mmol HBR_2, 1 mol% catalyst, 650 μl THF-d_8, 25 °C. [b] Yields were calculated *in situ* using hexamethylbenzene as an internal standard. [c] The TON numbers were calculated from the BBA yields.

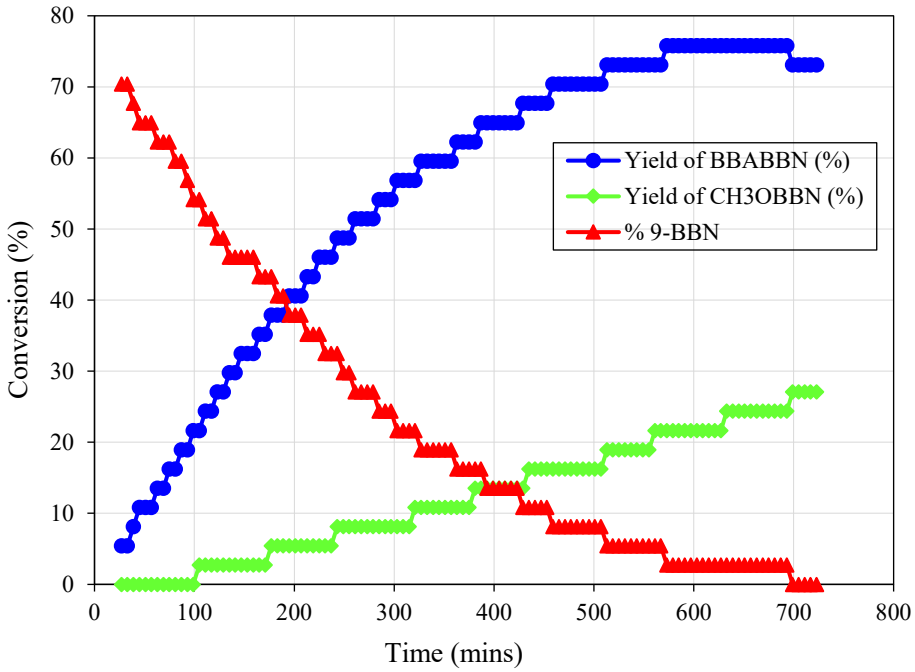

Figure S24: Plot of the evolution of reactant and products versus time in the hydroboration of CO_2 with 9-BBN with 1 mol-% of amidinato Mg hydride **3** (blue: bis(boryl)acetal, green methoxyborane, red: 9-BBN)

5.2. Hydrosilylation of CO_2 by hydrosilane catalyzed by Mg and Ca-based hydride complexes.

General procedure for NMR tube scale

In a glovebox, hydrosilane ($HSiR_3$) (0.13 mmol) and mesitylene (10 mol%, 0.013 mmol) as internal standard were added to a mixture of complex **3** (2 mol-%, 0.0028 mmol) and $B(C_6F_5)_3$ (0.013 mmol) in toluene-*d*$_8$ (0.55 ml) in a vial. The mixture was transferred to a pressurized NMR tube, which was sealed and removed from the glovebox. The sample was first degassed by freeze-pump-thaw and was then treated with CO_2 (1 atm). The conversion was monitored by ^1H and $^{13}C\{^1H\}$ NMR analyses at different time intervals. Products were identified by comparison with literature values. Yields of products and TON were determined by integration with respect to the mesitylene internal standard (Table S3).

Characteristic signals of products

Methane. **$^1H/^{13}C$ NMR** (300/100 MHz, 298 K, Toluene-*d*$_8$): δ 0.21 and -4.8 ppm.

Bis(silyl)acetal, $(Ph_3SiO)_2CH_2$. ^1H NMR (300 MHz, 298 K, Toluene-*d*$_8$): δ 7.67−7.64 (m, 12H, Ar−*H*), 7.24-7.12 (m, 18H, Ar−*H*), 5.46 (d, $^1J_{CH}$ = 164.39 Hz, 2H, *C*H_2). **$^{13}C\{^1H\}$ NMR** (101 MHz, 298 K, Toluene-*d*$_8$): δ 85.37 (s, *C*H_2).

Spectral data for **$(HPh_2Si)_2O$**. **^1H NMR** (300 MHz, 298 K, Toluene-*d*$_8$): δ 5.90 (s, 2H, Si−H), 7.05~7.14 (m, 12H, Ar−H), 7.57~7.60 (m, 8H, Ar−H).

Table S4: CO_2 hydrosilylation by [Mg]-based catalyst **3** with different hydrosilanes.

Hydrosilanes	time (h)	Si products (NMR% yield)[c]		TON[d] (TOF)/h^{-1})
$PhSiH_3$	2 h 40 min	CH_4 (26)	$(PhSiO_{1.5})_n$ (25%)	144(53.9)
Ph_2SiH_2	5 h 40 min	CH_4 (12)	$(HPh_2Si)_2O$ (44%)	105(18.6)
Ph_3SiH	220 h	$H_2C(OSiR_3)_2$ (97%)		50(0.3)

[a]Reaction condition: toluene-*d*$_8$ (0.1 ml, 298 K), $[Si{-}H]_0$ = 0.14 mmol, $[cat]_0$ = 0.0028 mmol (2 mol% per Si−H bond), $[B(C_6F_5)_3]$ = 0.014 mmol (10 mol% per Si−H), [M]/[B] = 1/5 ratio, $n(CO_2)_0$ = 1.3 x 10^{-4} mol (1 atm, 298 K), internal standard (mesitylene): 0.14 mmol. [b]The conversion of hydrosilane is determined by the integration of the ^1H NMR resonances vs. those of the standard, mesitylene. [c]Yield of the Si product is determined by the integration of the corresponding ^1H NMR peak vs. those of the standard, mesitylene. [d]TON number is calculated on the basis of Si−H bonds consumed per mmol of catalyst. TOF is calculated as TON h^{-1}. CH_4 yield is calculated as [mmol of reacted silane/4/(mmol of silane)] x 100. Si by product calculated in relation to the CH_4.

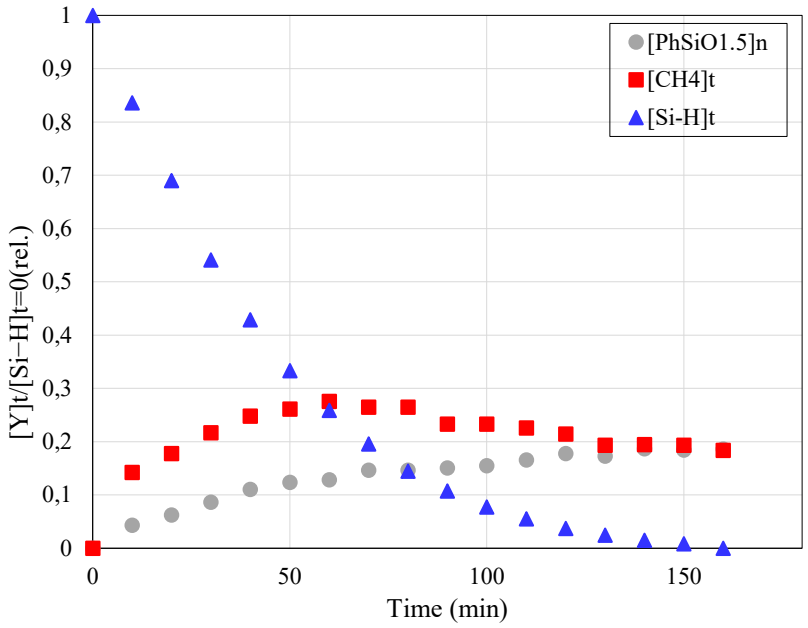

Figure S25: Plot of normalized reactant and product concentrations, $[Y]_t/[PhSiH_3]_{t=0}$ vs time [min] for reduction of CO_2 with $PhSiH_3$ under the following conditions: toluene-d_8 (0.1 mL), $[PhSiH_3]_0 = 0.14$ mmol, 2 mol% (0.0028 mmol) [**Mg (3)**]$_0$, 10 mol% (0.0035 mmol) $[B(C_6F_5)_3]_0$, $n(CO_2) = 1.3 \times 10^{-4}$ mol, internal standard (mesitylene) = 0.14 mmol; 25 °C.

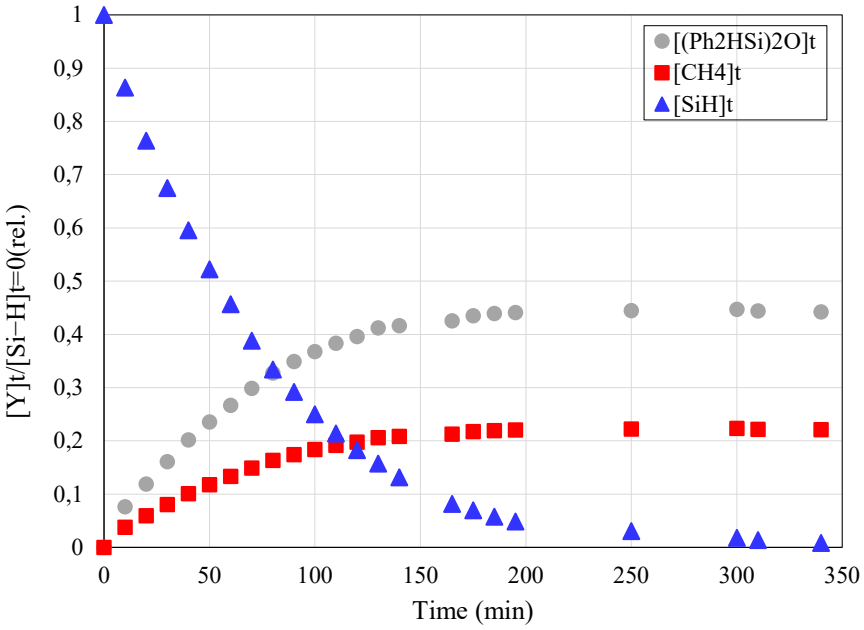

Figure S26: Plot of normalized reactant and product concentrations, $[Y]_t/[\ Ph_2SiH_2]_{t=0}$ vs time [min] for reduction of CO_2 with Ph_2SiH_2 under the following conditions: toluene-d_8 (0.1 mL), $[Ph_2SiH_2]_0 = 0.14$ mmol, 2 mol% (0.0028 mmol) [**Mg (3)**]$_0$, 10 mol% (0.0035 mmol) $[B(C_6F_5)_3]_0$, $n(CO_2) = 1.3 \times 10^{-4}$ mol, internal standard (mesitylene) = 0.14 mmol; 25 °C.